Longitudinal speed tracking control for a electric connected vehicle with actuator saturation subject to a replay attack

Xiang Li
Beihang University
Xiangyang Xu
Beihang University
Lu Chen (07398@buaa.edu.cn)
Beihang University School of Mechanical Engineering and Automation https://orcid.org/0000-0002-0389-5474
Hui Zhang
Beihang University
Zhiyang Ju
Beihang University
Wei Guo
Beihang University

Research Article

Keywords: Longitudianl speed tracking, Attack-induced time-varying delays, Actuator saturation, Nonlinear uncertainty, Anti-windup control

Posted Date: April 11th, 2022

DOI: https://doi.org/10.21203/rs.3.rs-1497118/v1

Nonlinear Dynamics manuscript No.
(will be inserted by the editor)

Longitudinal speed tracking control for a electric connected vehicle with actuator saturation subject to a replay attack

Xiang Li · Xiangyang Xu · Lu Chen · Hui Zhang · Zhiyang Ju · Wei Guo

the date of receipt and acceptance should be inserted later

Abstract In this paper, a delay-tolerable and anti-windup control synthesis technique is proposed. Longitudinal speed tracking performed by an integrated electric drive (IED) system under the multi-domain constraints of network bandwidth and actuator saturation is investigated. An in-vehicle controller area network (CAN) connect to the Internet providing an interface for cyber attacks which exacerbate network congestion. In addition, the physical saturation characteristics of the electric drive motor sacrifice vehicle speed tracking performance. Based on above problems, a nominal controller satisfying energy-to-peak performance considering the attack-induced delays is designed. Then, an augmented closed-loop system is established including the nominal delay-tolerable controller and an anti-windup controller considering input saturation and random attack-induced delays. The nonlinear uncertainty caused by attack-induced delay is described by polytopic inclusion. Furthermore, the saturation non-linearity is convert to sector-bounded uncertainty solved by linear matrix inequalities (LMIs) optimization. Particle swarm optimization (PSO) algorithm is employed to find the optimal anti-windup controller matrices. Finally, the effectiveness and superiority of the proposed method based on Matlab Simulink and hardware-in-the-loop (HiL) test platform are verified. The variation of speed tracking performance and oscillation damping capability under different attack energies is described.

Keywords Longitudianl speed tracking · Attack-induced time-varying delays · Actuator saturation · Nonlinear uncertainty · Anti-windup control

X. Li
The School of Transportation Science and Engineering, Beihang University, Beijing 100191, P.R. China
E-mail: Xiang_Li@buaa.edu.cn

X. Xu
The School of Transportation Science and Engineering, Beihang University, Beijing 100191, P.R. China
E-mail: xxy@buaa.edu.cn

L. Chen
The School of Mechanical Engineering and Automation, Beihang University, Beijing 100191, P.R. China
E-mail: 07398@buaa.edu.cn

H. Zhang
The School of Transportation Science and Engineering, Beihang University, Beijing 100191, P.R. China
E-mail: huizhang285@buaa.edu.cn

Z. Ju
The School of Transportation Science and Engineering, Beihang University, Beijing 100191, P.R. China
E-mail: zhiyangju@gmail.com

W. Guo
Ningbo Institute of Technology, Beihang University, Ningbo 315832, P.R. China
E-mail: guoweigreat@buaa.edu.cn

1 Introduction

The key assembly component of connected vehicles is the integrated electric drive (IED) system which is composed of drive motor and transmission device. The vehicle speed tracking performance performed by an IED system directly affects driving quality [7, 9, 39, 40]. With the development of electric vehicles and communication technologies, in-vehicle controller area network (CAN) connect to external networks providing drivers with more efficient, safe and enjoyable driving guidance [11, 22, 27, 34, 43]. Unfortunately, the wireless interfaces and malicious programs embedded in the in-vehicle network provide opportunities for attackers. Extensive vehicle attack experiments and in-vehicle network security protocol have been investigated [3, 10, 23, 24, 36]. Besides, Murvay et al. carried out a replay attack, a denial of Service (DoS) and a distributed DoS attack on commercial vehicles [26]. Kang et al. employed a CAN Analyzer

to carry out a deception attack [33]. Koscher et al. implemented a deception and a replay attack through on-board diagnostics (OBD) tool [16]. Han et al. have implemented a DoS attack, fuzzy attack, replay attack and malfunction software attack and unknown attack on in-vehicle CAN through an OBDII port and a simulation software CAN Test [12]. In addition, corresponding security protocols are also proposed. Woo et al. have carried out a remote replay attack on a vehicle through an OBDII and a malicious smartphone application [37]. However, resource limitations such as network bandwidth and finite computational ability may lead to in-vehicle communication network delay by processing large amounts of attack data.

However, the unknown random attack-induced delays on in-vehicle communication network may downgrade the real-time control performance. The design approaches of delay-tolerable controller in the study of [18–20, 41, 42, 46, 47] are proposed to mitigate the tracking performance degradation and powertrain oscillation of IED system under cyber attacks. Zhu et al. designed a speed tracking control technology for an IED system. The speed tracking performance of the system is guaranteed under CAN-induced delays [47]. Compared with CAN-induced delay, attack-induced delays have the characteristics of long time delay, random occurrence and random change of attack energy. An attack-delay robust controller described in the form of a dynamic output-feedback control was investigated [19]. An event-triggered controller to alleviate communication congestion in an attack network environment was studied [42]. Xu et al. proposed a robust reset control to optimize the speed tracking performance under attack-delays in real time [41]. However, attack-delay-tolerable controllers presented in generalized proportion integration (PI) form are sensitive to actuator saturation which may cause system unstable and device failure because of signal distortion [21, 44].

Based on above problems, this paper employs the indirect mitigation method of actuator saturation developed in [5, 6, 13, 28, 38], which is also known as anti-windup (AW) control method to improve the sensitivity of attack-delay-tolerable controllers to actuator saturation . For the consideration of economy and vehicle dynamic performance, the output torque of drive motor has inevitable physical limitation which affects the speed tracking performance and oscillation damping capability of an IED system. The integrator accumulates when input saturation happens resulting in more adjustment time and overshoot.In addition, stability analysis of closed-loop systems becomes more complicated when both delay and saturation exist in a control system. Therefore, it is imperative to design a robust anti-windup contrller to improve the tracking performance of the IED system under input saturation condition and ensure the control system stability under attack-delays. Theoretical methods considering input saturation and short time-delays have been investigated to reduce system conservatism [1, 2, 4, 8, 15, 17, 30, 32, 35, 45]. Muntazir et al. proposed a compensation control method for the state delay and input saturation nonlinear system, and proposed the conditions to ensure the local and global stability of the closed-loop system [15]. The stability region of the state delay system subject to input saturation was analyzed [31]. The stability conditions of linear matrix inequalities (LMIs) with and without time delay were obtained respectively. A robust anti-windup controller is proposed to solve the stability problem of time-varying delay system described by Takagi-Sugeno (T-S) fuzzy models. The stability condition is expressed by LMIs [25]. Hussain et al. proposed a solution method to compensate the controller for a system with time delay uncertainty, input nonlinearity, parameter uncertainty and additional disturbance [14]. In the literature, there are few studies on precise tracking control and driveline oscillation damping control under drive motor saturation condition. Zhang et al. studied multi-motor coordinated control of heavy-haul locomotive considering drive motor saturation [44]. Besides, there is little work to consider both attack-delays and actuator saturation for vehicle speed tracking control performed by IED systems.

Therefore, this paper proposes a vehicle speed tracking controller combing delay-tolerable and an anti-windup control to improve the speed tracking performance and powertrain oscillation damping capability considering actuator saturation under a replay attack. Furthermore, contributions of this paper are introduced: 1) A solving technology of delay-tolerable and anti-windup synthesis control based on particle swarm optimization (PSO) algorithm is developed, which is applied on vehicle speed tracking performed by an IED system. The PSO method is employed to assist in solving the optimization problems described by nonlinear matrix inequalities. 2) The experimental platform based on MATLAB and hardware-in-the-Loop (HiL) for simulating attack-delays is developed. The improvement and superiority of vehicle speed tracking performance and oscillation damping capability of the IED system against actuator saturation and a replay attack are verified compared with energy-to-peak controller and delay-tolerable controller designed by reference to [18]. 3) We describe the relationship between attack energy, bus load and in-vehicle network communication delays based on HiL tests. Furthermore, the effect of attack energy variation on vehicle speed tracking control with actuator saturation is investigated.

2 Problem formulation

2.1 Replay attack model

Fig. 1 shows a replay attack process, which is divided into vehicle speed tracking control and attacking [37].

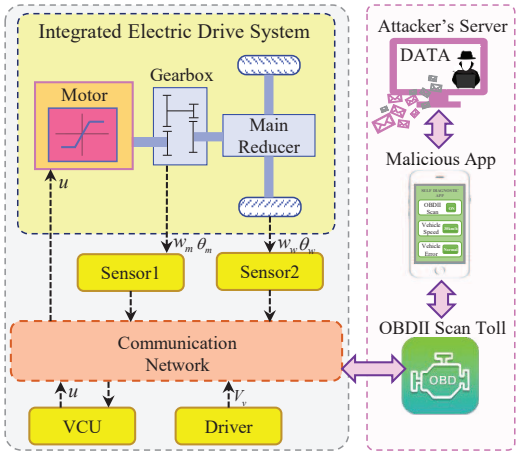

Fig. 1 The process of a replay attack on an IED system of a connected vehicle.

The key assembly of vehicle speed tracking IED system consists of a motor, a gearbox, a drive shaft, wheels, a vehicle control unit (VCU) and in-vehicle CAN. Sensor 1 collects signals of motor speed w_m and motor output angle θ_m. Sensor 2 collects signals of wheel speed w_w and wheel angle θ_w. The proposed control algorithm is downloaded into VCU to complete speed synchronization control. Furthermore, to realize the real-time observation of the vehicle status, an OBDII is embedded in the in-vehicle CAN through a physical interface. OBDII communicates with in-vehicle network eavesdroping and sending data at attacker's request, if the mobile application (APP) connected with OBDII by Bluetooth is malware designed by the attacker. This paper deals with the attack-induced delays after the work of [37].

2.2 Vehicle speed tracking system modeling

The expected speed V_x^* can be obtained by dividing the current pedal position by the maximum position and then multiplying by the maximum speed V_{max}. Furthermore, desired motor speed w_m^*, desired wheel speed w_w^* and desired motor output angle θ_m^*, desired motor torque T_m^* and desired external load torque T_{load}^* can be obtained through the following relations.

$$\begin{aligned} w_w^* &= V_x^*/r_w \\ w_m^* &= i_g i_0 w_w^*, \\ T_{load}^* &= k_f\theta_m^*/i_g i_0 - k_f\theta_w^* \\ T_m^* &= c_m i_g i_0 w_w^* + T_{load}^*/i_g i_0, \end{aligned} \tag{1}$$

Vehicle speed tracking is achieved through an IED system and the state space can be described by the following model [47].

$$\begin{aligned} \dot{x}_1 &= A_1 x_1 + B_1 u + E_1 w, \\ y_1 &= C_1 x_1, \end{aligned} \tag{2}$$

where

$$x_1 = \left[w_m - w_m^*, w_w - w_w^*, \left(\frac{\theta_m}{i_g i_0} - \theta_w\right) - \left(\frac{\theta_m^*}{i_g i_0} - \theta_w^*\right) \right]^{\mathrm{T}}$$

$$A_1 = \begin{bmatrix} -\frac{c_m}{J_{mg}} - \frac{c_f}{i_g{}^2 i_0{}^2 J_{mg}} & \frac{c_f}{i_g i_0 J_v} & -\frac{k_f}{i_g i_0 J_v} \\ \frac{c_f}{i_g i_0 J_v} & -\frac{c_a + c_f}{J_v} & \frac{k_f}{J_v} \\ \frac{1}{i_g i_0} & -1 & 0 \end{bmatrix}, C_1 = I,$$

$$B_1 = \left[\frac{1}{J_{mg}}, 0, 0 \right]^{\mathrm{T}}, E_1 = [I, -B_1], u = T_m, w = [d, T_m^*]^{\mathrm{T}},$$

with $x_1 \in \mathbb{R}^{n_{x_1}}$ is the state vector, $u \in \mathbb{R}^{n_u}$ is the control input, $w \in \mathbb{R}^{n_w}$ is the external input, and d is the modeling error between the mathematical model and the actual IED system, c_m is the motor damping, c_f is the driveshaft damping, k_f is the driveshaft stiffness, T_m is the motor torque, m_v is the vehicle mass, i_0 is the final drive ratio, i_g is the gear ratio, C_a is the air resistance coefficient, J_v is the vehicle inertia, J_g is the gearbox inertia, J_m is the motor inertia, w_g is the rotation speed of gearbox output shaft, w_m is the motor speed, w_w is the wheel speed, θ_w is the wheel angle, θ_m is the motor output angle, θ_g is the gearbox output shaft angle, T_{load} is the external load torque including air drag $T_{airdrag}$, rolling torque T_{roll} and resistant torque T_{grad} due to the road grade, r_w is the wheel radius, T_{gi} and T_{go} are the input and output torque of the gearbox, T_f is the driveshaft torque, and $\frac{w_m}{i_g i_0} - w_w$ is the axle wrap rate to evaluate powertrain jitter in engineering.

A new vector $x_2 = \left[x_1^{\mathrm{T}}, \int_0^t x_1^{\mathrm{T}} dt\right]^{\mathrm{T}}$ is employed to assist the design of the PI tracking controller. With the new vector, the IED model in (2) is rewritten as follows:

$$\begin{aligned} \dot{x}_2 &= A_2 x_2 + B_2 u + E_2 w, \\ y_2 &= C_2 x_2, \end{aligned} \tag{3}$$

where

$$A_2 = \begin{bmatrix} A_1 & 0 \\ I & 0 \end{bmatrix}, B_2 = \begin{bmatrix} B_1 \\ 0 \end{bmatrix}, E_2 = \begin{bmatrix} E_1 \\ 0 \end{bmatrix}, C_2 = C_1.$$

The continuous-time system in (3) is transformed into the following discrete-time model, considering that the sampled signal is sent periodically with sampling period T_s.

$$\begin{aligned} x_3(k+1) &= A_3 x_3(k) + B_3 u(k) + E_3 w(k), \\ y_3(k) &= C_3 x_3(k), \end{aligned} \tag{4}$$

where

$$A_3 = e^{A_2 T_s}, \; B_3 = \int_0^{T_s} e^{A_2(T_s-\theta)} d\theta \cdot B_2,$$

$$E_3 = \int_0^{T_s} e^{A_2(T_s-\theta)} d\theta \cdot E_2, \; C_3 = C_2.$$

2.3 Description of delay-tolerable system subject to attack-delays

Fig. 2 depicts the impact of an attack signal from an OBDII node the in-vehicle communication network.

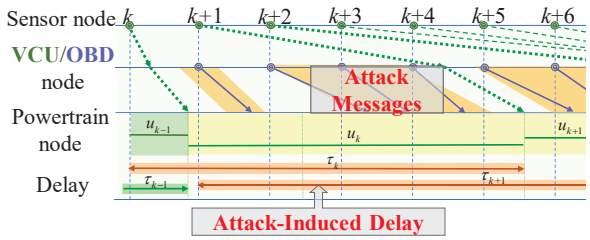

Fig. 2 The schematic diagram of data transmission under a replay attack.

Attackers replay higher-priority attack signals at a faster rate, resulting in random, long, time-varying, and unpredictable attack-delays. Assuming that the attack-induced random delays caused by attacks are bounded, and maximum delay $\tau_{\max}$ can be composed of ψT_s and ΥT_s as follows.

$$\tau_{\max} = (\psi + \Upsilon) T_s, \tag{5}$$

where $\psi \in Z_+$ and $\Upsilon \in R_{[0,1)}$. Therefore, the IED discrete-time system in (4) can be rewritten as the following nonlinear system considering the impact of attack-delays on actual control inputs.

$$\begin{aligned} x_3(k+1) = {} & A_3 x_3(k) + B_3 u(k) + E_3 \omega(k) \\ & + \Delta_{0,k}(u(k-1) - u(k)) + \cdots \\ & + \Delta_{\psi,k}(u(k-\psi-1) - u(k-\psi)), \end{aligned} \tag{6}$$

where

$$\Delta_{i,k} = \begin{cases} \int_0^{\tau_{k-i} - iT_s} e^{A_2(T_s-\theta)} d\theta \cdot B_2, & 0 \le \tau_{k-i} - iT_s \le T_s \\ \int_0^{T_s} e^{A_2(T_s-\theta)} d\theta \cdot B_2, & T_s \le \tau_{k-i} - iT_s \end{cases}$$

with $i = 0, 1, \cdots, \psi$. The nonlinear part in (6) can be linearized as follows by Taylor linear series expansion [29]. The h-order approximation of $\Delta(\varepsilon)$ is obtained by ignoring residual Θ^h. Therefore, nonlinear part $\Delta_{i,k}$ in (6) can be rewritten as follows.

$$\Delta_{i,k} = \begin{cases} \sum_{l=1}^{h+1} \beta_{i,l}(k) \widehat{R} \eta_{\Upsilon,l} B_2, \ \forall i = 0, 1, \cdots, \psi - 1 \\ \sum_{l=1}^{h+1} \beta_{i,l}(k) \widehat{R} \eta_{\psi,l} B_2, \ \forall i = \psi \end{cases} \tag{7}$$

where $\forall l = 1, 2, \cdots, h+1$, $\sum_{l=1}^{h+1} \beta_{i,l}(k) = 1$, $\beta_{i,l}(k) > 0$,

$$\widehat{R} = \left[0, \frac{(-1)^2}{1!} A_2^0 e^{A_2 T_s}, \cdots, \frac{(-1)^{h+1}}{(h)!} A_2^{h-1} e^{A_2 T_s} \right],$$

and

$$\eta_{\psi,l} = \begin{cases} \eta_{\psi,1} = [0\ 0\ \cdots\ 0]^{\mathrm{T}}, \\ \eta_{\psi,2} = [T_s\ 0\ \cdots\ 0]^{\mathrm{T}}, \\ \vdots \\ \eta_{\psi,h+1} = [T_s\ T_s^2\ \cdots\ T_s^h]^{\mathrm{T}}, \end{cases}$$

$$\eta_{\Upsilon,l} = \begin{cases} \eta_{\Upsilon,1} = [0\ 0\ \cdots\ 0]^{\mathrm{T}}, \\ \eta_{\Upsilon,2} = [(\Upsilon T_s)\ 0\ \cdots\ 0]^{\mathrm{T}}, \\ \vdots \\ \eta_{\Upsilon,h+1} = [(\Upsilon T_s)\ (\Upsilon T_s)^2\ \cdots\ (\Upsilon T_s)^h]^{\mathrm{T}}. \end{cases}$$

Therefore, defining a new state vector $x_4(k) = [x_3^{\mathrm{T}}(k), u^{\mathrm{T}}(k-1), \cdots, u^{\mathrm{T}}(k-\psi-1)]^{\mathrm{T}}$, the nonlinear system in (6) can be reformulated to the following state-space model:

$$x_4(k+1) = A_4(\alpha) x_4(k) + B_4(\alpha) u(k) + E_4 \omega(k), \tag{8}$$

where

$$A_4(\alpha) = \begin{bmatrix} A_3 & \Delta_{0,k} - \Delta_{1,k} & \cdots & \Delta_{\psi-1,k} - \Delta_{\psi,k} & \Delta_{\psi,k} \\ 0 & 0 & \cdots & 0 & 0 \\ 0 & I & \cdots & 0 & 0 \\ \vdots & \vdots & \ddots & \vdots & \vdots \\ 0 & 0 & \cdots & I & 0 \end{bmatrix}$$

$$B_4(\alpha) = \begin{bmatrix} B_3 - \Delta_{0,k} \\ I \\ 0 \\ \vdots \\ 0 \end{bmatrix}, \quad \text{and} \quad E_4 = \begin{bmatrix} E_3 \\ 0 \\ 0 \\ \vdots \\ 0 \end{bmatrix}.$$

3 Nominal delay-tolerable controller solving

The design objective of the nominal delay-tolerable controller is to track the ideal vehicle speed and increase oscillation damping capability. Therefore, the weighted sum of the wheel speed error and wheel angle error are chosen as the first control output Z_1, the axle wrap rate is selected as the control output Z_2 which is shown as follows.

$$\begin{aligned} Z_1(k) = {} & G_1 x_4(k), \\ Z_2(k) = {} & G_2 x_4(k), \end{aligned} \tag{9}$$

where $G_1 = [0, \chi_1, 0, 0, \chi_2, 0, \underbrace{[0, \cdots, 0]}_{r+1}]$, $G_2 = [-\frac{I}{i_g i_0}, -I, 0, 0, 0, 0, \underbrace{[0, \cdots, 0]}_{r+1}]$, with χ_1 and χ_2 are the weighting factors between wheel speed error and wheel angle error. The nominal control law is designed as $u(k) = K_{nom} x_4(k)$. Modeling error and attack-induced delays are considered as external disturbances in the design of nominal delay-tolerable controller. The following lemma is introduced to guarantee the

stability of system in (8) and energy-to-peak performance ignoring input saturation.

Lemma 1: [47] Suppose that the nominal delay-tolerable controller is designed. The nominal closed-loop system is stable with energy-to-peak performance indexes ϑ_1 and ϑ_2, if there exist a positive definite matrix $\xi = \xi^{\mathrm{T}}$, and matrices M and Y satisfying the following conditions

$$\begin{bmatrix} -\xi & A_4(\alpha)\xi + B_4(\alpha)Y & E_4 \\ * & \xi - M - M^{\mathrm{T}} & 0 \\ * & * & -I \end{bmatrix} < 0, \tag{10}$$

$$\begin{bmatrix} -\xi & \xi G_1^{\mathrm{T}} \\ * & -\vartheta_1^2 I \end{bmatrix} < 0, \tag{11}$$

$$\begin{bmatrix} -\xi & \xi G_2^{\mathrm{T}} \\ * & -\vartheta_2^2 I \end{bmatrix} < 0. \tag{12}$$

There are two performance parameters ϑ_1 and ϑ_2 in Lemma 1. Speed tracking performance with the smaller wrap rate is expected to obtained better oscillation damping capability. Therefore, the nominal tracking controller gain is solved by following optimal problem.

$$\begin{aligned} &\min_{\xi, M, Y, \vartheta_1, \vartheta_2} \ \vartheta_2^2 I, \\ &\text{subject to } (10) - (12). \end{aligned} \tag{13}$$

Each item $\Delta_{i,k}$ generates $h+1$ terms as shown in (7) and $\psi+1$ uncertain terms $\Delta_{0,k}, \Delta_{1,k}, \cdots, \Delta_{\psi,k}$ exist. Furthermore, the system in (8) is described by following $(h+1)^{\psi+1}$ systems, because there are $(h+1)^{\psi+1}$ convex polytope vertices describing the uncertain terms, i.e., [29, 47]

$$\begin{aligned} x_4(k+1) = \tilde{A}_{4,i} x_4(k) + \tilde{B}_{4,i} u(k) + E_4 \omega(k), \\ \forall i = 1, 2, \ldots, (h+1)^{\psi+1}. \end{aligned} \tag{14}$$

Therefore, the condition in (10) is further developed as follows to find optimal nominal control gain K_{nom}.

$$\begin{aligned} &\begin{bmatrix} -\xi & \tilde{A}_{4,i}\xi + \tilde{B}_{4,i}Y & E_4 \\ * & \xi - M - M^{\mathrm{T}} & 0 \\ * & * & -I \end{bmatrix} < 0, \\ &\forall i = 1, 2, \cdots (h+1)^{\psi+1}. \end{aligned} \tag{15}$$

Once the minimization problem in (13) is solved, the nominal tracking controller gain can be obtained by $K_{nom} = Y\xi^{-1}$.

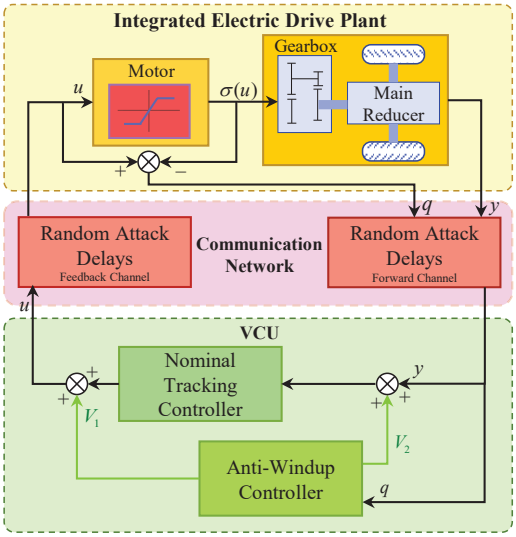

Fig. 3 Schematic diagram of the augmented closed-loop system for IED speed tracking control under random attack delays and input saturation.

4 Anti-windup compensation

4.1 Delay-tolerable control with anti-windup compensation

This section presents the design method of the closed-loop control system considering attack-induced delays and input saturation. Fig. 3 shows the IED system communicating with the VCU over in-vehicle CAN. The nominal tracking controller and anti-windup controller are downloaded into VCU. The anti-windup controller actions when input saturation is detected.

The nonlinear properties of input saturation can be described by piecewise linear saturation function as follows.

$$\sigma(u_i) = \begin{cases} u_i, & |u_i| \le u_i^{max} \\ \mathrm{sgn}(u_i) u_i^{max}, & |u_i| > u_i^{max} \end{cases} \tag{16}$$

for $i = 1, 2, \ldots, n_u$. The relationship between nominal control input $u(k)$ and saturated control input $\sigma(u(k))$ can be expressed as follows.

$$q(k) = u(k) - \sigma(u(k)), \tag{17}$$

where $q(k)$ is the difference connecting the uncertainty caused by input saturation. The anti-windup control structure diagram is shown in Fig. 3. Then, the anti-windup controller is described by following equations [13, 38].

$$\begin{bmatrix} x_{\mathrm{aw}1}(k+1) \\ x_{\mathrm{aw}2}(k+1) \\ V_1(k) \\ V_2(k) \end{bmatrix} = \begin{bmatrix} A_{aw} & 0 & B_{aw} \\ 0 & A_1 & B_1 \\ C_{aw} & 0 & D_{aw} \\ 0 & C_1 & D_1 \end{bmatrix} \begin{bmatrix} x_{aw1}(k) \\ x_{aw2}(k) \\ q(k) \end{bmatrix}. \tag{18}$$

where A_{aw}, B_{aw}, C_{aw} and D_{aw} is the anti-windup controller matrices, $x_{aw1}(k)$ and $x_{aw2}(k)$ are the state vectors of the anti-windup controller, $V_1(k)$ and $V_2(k)$ are outputs of the anti-windup controller which are used to modify the output and the input of the nominal controller, respectively. Furthermore, the combined controller gain is rewritten as follows by combining the nominal delay-tolerable controller with the anti-windup controller.

$$u(k) = K_{nom}\left[x_4(k) - HV_2(k)\right] + V_1(k), \tag{19}$$

where $H = \left[I_{n_{x1}\times n_{x1}}, 0_{(n_{x1}+n_u)\times n_{x1}}\right]^{\mathrm{T}}$ is the expanded matrix.

4.2 Integrated closed-loop system of delay-tolerable controller and anti-windup controller

The final closed-loop system considering control input saturation and attack-induced delays can be expressed as follows.

$$x_4(k+1) = A_4(\alpha)x_4(k) + B_4(\alpha)\sigma(u(k)) + E_4 w(k), \tag{20}$$

The control objective of the final closed-loop system is to balance tracking errors with control inputs considering attack-induced delays and input saturation. Therefore, the following linear quadratic regulator (LQR) indicator Φ is employed as the controlled output Z_3 of the argument closed-loop system.

$$\Phi = \sum_{k=0}^{\infty}\left(e^{\mathrm{T}}(k)Qe(k) + \sigma(u)^{\mathrm{T}}(k)R\sigma(u(k))\right). \tag{21}$$

The LQR performance can be further translated into a two norm of the control output $Z_3(k)$ as shown below.

$$Z_3(k) = F_4 x_4(k) + G_4\sigma(u(k)) - G_4 q(k), \tag{22}$$

where $F_4 = \begin{bmatrix} 0 & Q^{\frac{1}{2}} & \dots & 0 & 0 \\ 0 & 0 & \dots & 0 & 0 \end{bmatrix}, G_4 = \begin{bmatrix} 0 \\ R^{\frac{1}{2}} \end{bmatrix}$.

Denoting $x_5(k) = \left[x_4^{\mathrm{T}}(k), x_{aw1}^{\mathrm{T}}(k), x_{aw2}^{\mathrm{T}}(k)\right]^{\mathrm{T}}$. Therefore, the augmented closed-loop system is designed as follows:

$$\begin{bmatrix} x_5(k+1) \\ u(k) \\ Z_3(k) \end{bmatrix} = \begin{bmatrix} A_5(\alpha) & B_5(\alpha) & E_5 \\ C_5 & D_5 & 0 \\ F_5 & G_5 & 0 \end{bmatrix} \begin{bmatrix} x_5(k) \\ q(k) \\ w(k) \end{bmatrix} \tag{23}$$

where

$$A_5(\alpha) = \begin{bmatrix} \Gamma_1 & B_4(\alpha)C_{aw} & \Gamma_2 \\ 0 & A_{aw} & 0 \\ 0 & 0 & A_1 \end{bmatrix},\ B_5(\alpha) = \begin{bmatrix} \Gamma_3 \\ B_{aw} \\ B_1 \end{bmatrix},$$
$$E_5 = \left[E_4^{\mathrm{T}}, 0, 0\right]^{\mathrm{T}},\ C_5 = \left[K_{nom}, C_{aw}, -K_{nom}HC_1\right],$$
$$D_5 = -K_{nom}HD_1 + D_{aw},$$
$$F_5 = \left[F_4 + G_4K_{nom}, G_4C_{aw}, -G_4K_{nom}HC_1\right],$$
$$G_5 = -G_4 - G_4K_{nom}HD_1 + G_4D_{aw},$$
$$\Gamma_1 = A_4(\alpha) + B_4(\alpha)K_{nom},\ \Gamma_2 = -B_4(\alpha)K_{nom}HC_1,$$
$$\Gamma_3 = -B_4(\alpha) - B_4(\alpha)K_{nom}HD_1 + B_4(\alpha)D_{aw}.$$

5 Solving algorithm for PSO-AW controller

In this section, an nonlinear anti-winup controller solving method based on PSO algorithm is developed, also called as PSO-AW controller. The PSO algorithm is used to assist optimization problem expressed by nonlinear matrix inequalities. Finally, the anti-windup controller matrices are obtained for offline calculation.

5.1 Fitness Function Definition

In this section, the nonlinear problem caused by motor saturation is described by a kind of uncertain system with sector-bounded uncertainty [13, 38]. The uncertainties q caused by actuator saturation contained in a conic sector $[0, k_i], i = 1, 2, ..., n_u$ which defined by $q \in \mathrm{sect}[0, L]$ will indirectly restrict the control input signal, where $L = \mathrm{diag}\{k_1, k_2, \dots, k_{n_u}\}$ and $0 < k_i < 1$. Then, regional stability will be achieved. The limitations of saturated non-linearity can then be described as the following constraints:

$$q^{\mathrm{T}}(k)W(Lu(k) - q(k)) \geq 0, \tag{24}$$

for any diagonal matrix $W = diag\{\varpi_1, \varpi_2, \dots, \varpi_{n_u}\}$. Suppose that the argument closed-loop system in (23) is designed. The following Theorem 1 introduces the methods and conditions for solving the anti-windup controller matrices.

Theorem 1: The closed-loop system in (23) is asymptotically stable satisfying H_∞ performance indexes γ which against the saturation uncertainty $q \in \mathrm{sect}[0, L]$, if positive definite diagonal matrix W, positive definite matrix $\Omega = \Omega^{\mathrm{T}}$, M and matrices A_{aw}, B_{aw}, C_{aw} , D_{aw} with appropriate dimensions satisfying

$$\begin{bmatrix} -\Omega & 0 & \tilde{A}_{5,i}J & \tilde{B}_{5,i} & E_5 \\ * & -\gamma I & F_5 J & G_5 & G_5^* \\ * & * & \Omega - J - J^{\mathrm{T}} & \Omega \Xi_1 & 0 \\ * & * & * & \Xi_2 & 0 \\ * & * & * & * & -\gamma I \end{bmatrix} < 0, \quad \forall i = 1,2,\cdots (h+1)^{\psi+1}, \tag{25}$$

where

$$\tilde{A}_{5,i} = \begin{bmatrix} \Lambda_{1,i} & \tilde{B}_{4,i}C_{aw} & \Lambda_{2,i} \\ 0 & A_{aw} & 0 \\ 0 & 0 & A_1 \end{bmatrix},\ \tilde{B}_{5,i} = \begin{bmatrix} \Lambda_{3,i} \\ B_{aw} \\ B_1 \end{bmatrix},$$
$$\Xi_1 = C_5^{\mathrm{T}} L^{\mathrm{T}} W^{\mathrm{T}},\ \Xi_2 = WLD_5 + D_5^{\mathrm{T}} L^{\mathrm{T}} W^{\mathrm{T}} - 2W,$$
$$\Lambda_{1,i} = \tilde{A}_{4,i} + \tilde{B}_{4,i} K_{nom},\ \Lambda_{2,i} = -\tilde{B}_{4,i} K_{nom} H C_1,$$
$$\Lambda_{3,i} = -\tilde{B}_{4,i} - \tilde{B}_{4,i} K_{nom} H D_1 + \tilde{B}_{4,i} D_{aw}.$$

Proof: Sufficient conditions to satisfy the asymptotic stability of the uncertain system in (23) considering H_∞ performance are established as follows:

$$\begin{aligned} \Psi =& \varepsilon \{V_{k+1} \mid x_5(k)\} - x_5^{\mathrm{T}}(k) S x_5(k) \\ &+ q^{\mathrm{T}}(k) W (Lu(k) - q(k)) \\ &+ \frac{1}{\gamma} Z(k)^{\mathrm{T}} Z(k) - \gamma w(k)^{\mathrm{T}} w(k) < 0, \end{aligned} \tag{26}$$

since

$$\begin{aligned} &\varepsilon \{V_{k+1} \mid x_5(k)\} \\ &= \varepsilon \{x_5(k+1)^{\mathrm{T}} S x_5(k+1)\} \\ &= \begin{bmatrix} x_5(k) \\ q(k) \\ w(k) \end{bmatrix}^{\mathrm{T}} \begin{bmatrix} A_5^{\mathrm{T}}(\alpha) \\ B_5^{\mathrm{T}}(\alpha) \\ E_5^{\mathrm{T}} \end{bmatrix} S [A_5(\alpha), B_5(\alpha), E_5] \begin{bmatrix} x_5(k) \\ q(k) \\ w(k) \end{bmatrix}, \end{aligned} \tag{27}$$

based on (23),

$$Z_3^{\mathrm{T}}(k) Z_3(k) = \begin{bmatrix} x_5(k) \\ q(k) \\ w(k) \end{bmatrix}^{\mathrm{T}} \begin{bmatrix} F_5^{\mathrm{T}} \\ G_5^{\mathrm{T}} \\ 0 \end{bmatrix} [F_5, G_5, 0] \begin{bmatrix} x_5(k) \\ q(k) \\ w(k) \end{bmatrix}. \tag{28}$$

The constraint conditions in (24) can be further expressed as follows:

$$\begin{aligned} &2q^{\mathrm{T}}(k) W (Lu(k) - q(k)) \\ &= \begin{bmatrix} x_5(k) \\ q(k) \\ w(k) \end{bmatrix}^{\mathrm{T}} \begin{bmatrix} 0 & \Xi_1 & 0 \\ * & \Xi_2 & 0 \\ * & * & 0 \end{bmatrix} \begin{bmatrix} x_5(k) \\ q(k) \\ w(k) \end{bmatrix}, \end{aligned} \tag{29}$$

Therefore, the condition in (26) can be expressed by following matrix inequality by applying Schur complement:

$$\begin{bmatrix} -S^{-1} & 0 & A_5(\alpha) & B_5(\alpha) & E_5 \\ * & -\gamma I & F_5 & G_5 & 0 \\ * & * & -S & \Xi_1 & 0 \\ * & * & * & \Xi_2 & 0 \\ * & * & * & * & -\gamma I \end{bmatrix} < 0. \tag{30}$$

In the reference of [47], define $\Omega = S^{-1}$ and apply a congruence transformation to (30) with diag $\{I, I, S^{-1}, I, I\}$, the nonlinear matrix inequality in (30) can be described by (25) by polytopic inclusion method. Therefore, the Proof is thereby completed. ■

However, the matrix inequalities in (25) cannot be solved directly because of the bilinear term $\tilde{A}_{5,i}J$ and $F_5 J$, $\forall i = 1,2,\cdots (h+1)^{\psi+1}$. Therefore, PSO is employed to assist Theorem 1 to derive the anti-windup controller matrices.

5.2 Searching algorithm of PSO-AW controller matrices

This section presents a searching method for optimal or near optimal anti-windup controller matrices A_{aw}, B_{aw}, C_{aw} and D_{aw} with PSO algorithm. Each particle P_j contains the matrix elements in A_{aw}, B_{aw}, C_{aw}, D_{aw}. Therefore, the particle P_j stands for $A_{aw,j}$, $B_{aw,j}$, $C_{aw,j}$ and $D_{aw,j}$, where j is the particle number, $\forall j = 1,2,\ldots,N_1$, and N_1 is the total number of particles. The solving method is introduced below.

Step 1): Specify the boundary of the PSO optimization problem. Particles position $P_j(n)$ and velocity $V_j(n)$ are restricted as follows which are calculated by pole assignment.

$$\begin{aligned} &P_j(n) \in [P_{\min}, P_{\max}], j = 1,2,\ldots,N_1, \\ &V_j(n) \in [V_{\min}, V_{\max}], n = 0,1,\ldots,N_2, \end{aligned} \tag{31}$$

where n is the iteration step and N_2 is the total number of iterations.

Step 2): A set of feasible solutions satisfying matrix inequalities in (25) are employed as the initialization position of particles $P_j(0) = \{A_{aw,j}(0), B_{aw,j}(0), C_{aw,j}(0), D_{aw,j}(0)\}$, $\forall j = 1,2,\ldots,N_1$. Initialize randomly the individuals velocities $V_j(0)$.

Step 3): Particle velocity and position are updated. The following equations describe the method to update the position and velocity of particles.

$$\begin{aligned} &Y_j(n+1) = Y_j(n) + V_j(n+1), \\ &V_j(n+1) = c_3 V_j(n) + c_1 r_{a1} \left(P_j^{pb}(n) - P_j(n) \right) \\ &\qquad + c_2 r_{a2} \left(P^{gb}(n) - P_j(n) \right), \end{aligned} \tag{32}$$

$\forall n = 1,2,\cdots,N_2$, where N_2 is the maximum iteration number, c_3 is the inertia weight, c_1 and c_2 are the accelerated

constant, r_{a1} and r_{a2} are the random numbers drawn from 0 to 1, $P_j^{pb}(n)$ is the best position in the nth iteration.

Step 4): Calculate the fitness function given by following optimization problem with $A_{aw,j}$, $B_{aw,j}$, $C_{aw,j}$ and $D_{aw,j}$ as known.

$$\min_{W_j,\Omega_j,J_j} \gamma_j, \text{subject to } (25). \tag{33}$$

The particles with the best fitness function are selected as the local optimal solution represents the optimal H_∞ performance index γ. $P^{gb}(n)$ is the optimal position of all particles up to the nth iteration, which is remembered as the global best position.

Step 5): After N_2 iterations, the optimal particles can be obtained as $P = P^{gb}(N_2)$.

Therefore, the theoretical feasibility of control synthesis technology considering attack-delays and actuator saturation is analyzed. Then, the proposed method is fully verified by simulation attacks based on MATLAB and real attack based on HiL.

6 Simulation results

The improvement of the proposed method is studied. Simulations are carried out based on MATLAB Simulink (R2018b, MathWorks, USA) platform compared with a delay-tolerable algorithm designed by reference of [18]. The IED control system shown in Fig. 3 is used as a simulation framework. The proposed method is encapsulated in the VCU to calculate desired motor torque. The saturation function of motor module limits the actual output torque to 130Nm. Attack-induced delays are simulated with the network module in MATLAB. The sampling time is set at 20ms.

The main parameters of an IED are listed in Table I. The controller and the parameters are listed below. The nominal delay-tolerable controller gain solved by Corollary 1 is $K_{nom} = [-0.10, -32.47, 160.40, 0.00, -0.76, -0.00, -0.02, 0.02]$, with $\chi_1 = 1$, $\chi_2 = 200$, $\vartheta_1 = 0.0023$, $\vartheta_2 = 15$.

The gain matrices of anti-windup controller solved by PSO-AW are

$$A_{aw} = \begin{bmatrix} 0.31 & 6.63 & -353.07 \\ 0.01 & 0.98 & 1.02 \\ 0.01 & -0.02 & 0.69 \end{bmatrix}, B_{aw} = \begin{bmatrix} 0.56 \\ 0.02 \\ 0.01 \end{bmatrix}$$

$$C_{aw} = [-0.62, 0.63, -0.66], \quad \text{and} \quad D_{aw} = -3.$$

with $\gamma = 0.033$, $N_1 = 16$, $N_2 = 100$, $c_1 = 2$, $c_2 = 2$, $Q = \text{diag}\{1, 10, 0\}$, $R = 1$.

In order to verify the improvement performance of the proposed algorithm in speed tracking and oscillation damping. The comparative simulation of the proposed controller and delay-tolerable controller is performed under input saturation and random delays with maximum 100ms. Fig. 4 (a)-(d) show the response of vehicle speed, motor torque, wrap rate and driveshaft torque. We can see from Fig. 4 (a) that the proposed controller reduces the effect of actuator saturation. Better speed synchronization performance with smaller overshoot and steady-state time, even under attacks. Fig. 4 (b) shows the motor actual output torque of delay-tolerable controller fluctuates more. Vibration reduces powertrain life and provides poor ride comfort. Fig. 4 (c) shows the comparison of axle wrap rate responses of two controllers. Greater jitter of delay-tolerable controller during gear shift can be seen, while the proposed controller has smaller peaks and jitter. It indicates that the oscillation damping capability is improved.

Table 1 Key Parameters of IED System.

Symbol	Meaning	Value
m_v	Vehicle mass	1094kg
i_0	Final drive ratio	3.667
i_g	Gear ratio	3.778
C_a	Air resistance coefficient	2.7N·m·s/rad
k_f	Driveshaft stiffness	6000 N·m/rad
c_f	Driveshaft damping	42N·m·s/rad
c_m	Motor damping	0.15N·m·s/rad
J_w	Wheels inertia	5.38kg·m^2
J_g	Gearbox inertia	1.1828kg·m^2
J_m	Motor inertia	0.01kg·m^2
r_w	Wheel rolling radius	0.281m

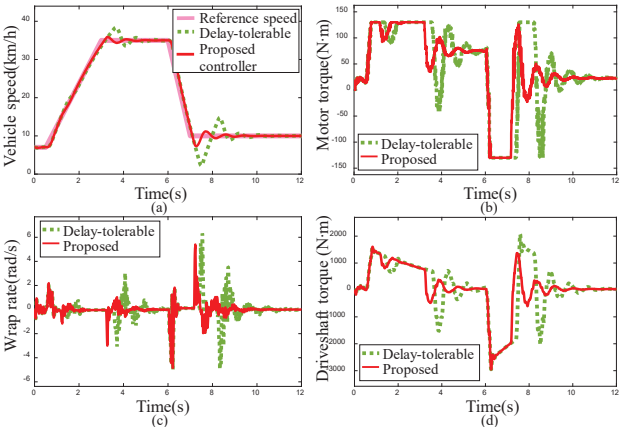

Fig. 4 The performance of anti-windup control under a random replay attack.

7 HiL test results

The effectiveness and superiority of the proposed method is studied in this section. Experimental verification based on the HiL platform is employed as shown in Fig. 5. The hardware equipment includes two personal computers (PCs) named PC 1 and PC 2, a VCU, a Vector VN1640A CAN interface, a driver pedal, a dSPACE and a practical CAN bus. The baud rate of the CAN bus is 500kBuad. PC 1 runs Matlab Simunlink and ControlDesk. PC 2 runs Matlab/Simunlink

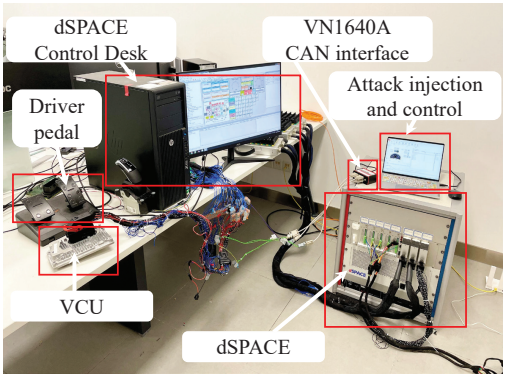

Fig. 5 HiL experimental platform physical picture.

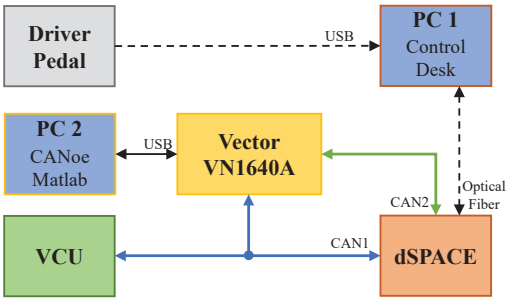

Fig. 6 HiL experimental platform schematic diagram.

and CANoe. Under the control of PC 2, Vector VN1640A added attack messages into CAN bus. Moreover, the schematic diagram of the HiL is shown in Fig. 6. The IED model is downloaded into dSPACE. The proposed control algorithm is downloaded into VCU by PC 1.

Messages from the IED system and VCU are transmitted on a 20ms cycle. CAN bus load and communication delay are important indexes to measure communication quality, is used to describe the attack energy in this section. The root mean square error (RMSE) index is applied to evaluate the control system tracking effect.

7.1 Verification of effectiveness and superiority under HiL Test

In this section, the proposed delay-tolerable and anti-windup synthesis controller are compared with an energy-to-peak controller without considering delay and actuator saturation and a delay-tolerable controller designed with reference to [18]. The IED system in Fig. 1 is built in dSpace. The above three control algorithms are built in an actual VCU to track the step speed signal from 0km/h-30km/h. A set of attack messages with random transmission cycles are designed in CANoe to simulate replay attacks under a security protocol framework. The transmission period of the attack messages is randomly selected from 4ms to 10ms. The response of

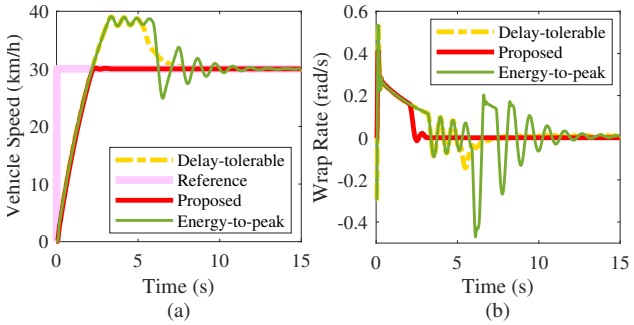

Fig. 7 Comparisons of speed tracking and oscillation damping performance under 10 attack messages in the presence of actuator saturation: (a) Vehicle speed, (b) Wrap rate.

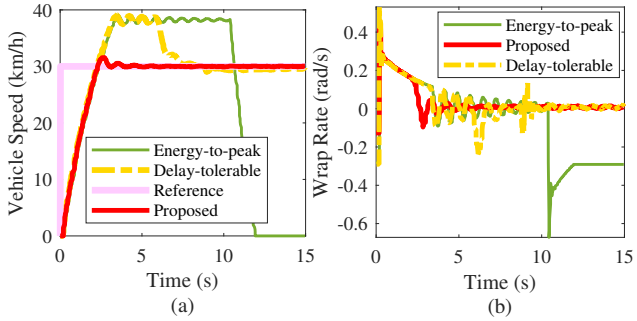

Fig. 8 Comparisons of speed tracking and oscillation damping performance under 25 attack messages in the presence of actuator saturation: (a) Vehicle speed, (b) Wrap rate.

speed tracking and wrap rate with 10 attack messages and 25 attack messages are shown in Fig. 7 and Fig. 8.

Fig. 7(a) shows the response of speed tracking. The speed response of energy-to-peak controller has the largest overshoot, and delay-tolerable second. The proposed controller has smallest overshoot and reaches steady state fastest. Actuator saturation causes the integral module of the controller to accumulate, due to the performance of delay-tolerable controller reduced. Energy-to-peak controller has the worst performance due to the combined effect of actuator saturation and attack-delays. Therefore, the proposed controller has the best speed tracking performance under the condition of actuator saturation with the presence of 10 attack messages. Fig. 7(b) shows the response of wrap rate. Energy-to-peak controller has the largest jitter, followed by delay-tolerable controller and proposed controller. The wrap rate of the IED system under proposed controller reaches steady state first. This means that the proposed control has the best oscillation damping capability under the condition of actuator saturation and 10 attack messages.

Fig. 8(a) shows the speed tracking responses. The speed of the IED system under energy-to-peak control reaches about 38km/h in 3s, and the speed dropped to 0km/h after 11.9s. Therefore, we can see from that the energy-to-peak controller lost its control ability. The overshoot appears under

the control of delay-tolerable controller, and there are fluctuations and steady-state errors in the steady state. The proposed controller reaches steady state first. We can conclude that under the condition of 25 attack messages and actuator saturation, the proposed controller has the best speed tracking performance. Fig. 8(b) shows the wrap rate responses. The proposed controller reaches steady state first. Then the delay-tolerable controller reaches. The energy-to-peak controller maintains -2.91 after 11.9s. It means that the powertrain system continues to vibrate. It is seen from Fig. 8(a) that the energy-to-peak controller loses its control ability, and the vehicle is in a dangerous state under this test condition. However, the proposed controller show its superiority in oscillation damping.

7.2 The influence of attack energy variation on speed tracking performance and oscillation damping capability

In this section, the RMSE values of speed tracking and wrap rate of the three controllers are counted under varying attack energy. The magnitude of attack energy is represented by amount of attack messages with random transmission period from 4ms to 10ms. The average delay is the average value of the attack-delays measured by the CAPL program of CANoe. Average bus load is calculated by the average value of real-time bus load obtained by CANoe.

The relationship of average delay with the amount of attack message can be seen from Fig. 9(a) and and Table 2. It can be seen that the amount of attack messages is positively correlated with the average bus load. According to the experimental results, 25 attack messages lead to a 100% bus load under this test condition. More attack messages cause the IED system bus-off and a DoS occurs. Fig. 9(b) and Table 3 show that the speed RMSE values of the three methods are increasing, but energy-to-peak keeps largest, the delay-tolerable is the second, and the proposed method has the smallest speed RMSE value. This means that proposed method has the lowest sensitivity to the increase attack messages. Moreover, the proposed method not only has the best speed tracking effect under different bus load, but also has the strongest stability against bus load and communication delay changes. Delay-tolerable method is second. Energy-to-peak controller has the worst tracking performance and the highest sensitivity to communication delay changes. As can be seen from Fig. 9(c) and Table 4, the RMSE value of wrap rate of energy-to-peak controller keeps increasing with attack messages. When the delay is less than 4.551ms, the RMSE value of proposed method have barely changed. In addition, the RMSE value of delay-tolerable method hardly changes when the communication delay is less than 1.418ms. While the values gradually increase when the attack messages increases to more than 20. We can conclude that when the bus load rate exceeds 81.93%, the communication delay surges, which has a great impact on the tracking effect.

Table 2 The Relationship between Attack Energy and Attack Messages.

Attack energy	Attack messages					
	0	5	10	15	20	25
Average bus load (%)	4.17	22.41	42.51	61.72	81.93	100
Average delay (ms)	0.01	0.04	0.52	1.42	4.55	60.80

Table 3 RMSE Values of Speed Tracking.

Controller name	Attack messages					
	0	5	10	15	20	25
Energy-to-peak	7.23	7.25	7.26	7.27	7.31	17.02
Proposed	6.19	6.19	6.20	6.21	6.23	6.43
Delay-tolerable[18]	7.02	7.03	7.03	7.04	7.07	7.38

Table 4 RMSE Values of Wrap Rate.

Controller name	Attack messages					
	0	5	10	15	20	25
Energy-to-peak	0.14	0.14	0.14	0.14	0.14	0.21
Proposed	0.08	0.08	0.08	0.08	0.08	0.09
Delay-tolerable[18]	0.10	0.10	0.10	0.10	0.10	0.11

8 Conclusions

In this work, a delay-tolerable and anti-windup control synthesis technique with good robustness against attack-induced random delays and input saturation has been proposed for vehicle speed tracking control. Simulation maneuver subjected to random attack-delays is carried out based on Matlab/Simulink to verify the effectiveness and superiority of the proposed controller. Simulation results show that the proposed method achieves good speed tracking performance with less powertrain vibration compared with delay-tolerable controller designed by the reference of [18]. HiL tests are carried out at different attack energies compared with delay-tolerable controller in [18] and energy-to-peak controller in step speed tracking conditions from 0km/h to 30km/h. The results of HiL test are summarized as follows: 1) The amount of attack messages is proportional to the bus load and the rate of change of the communication delays. 2) The RMSE

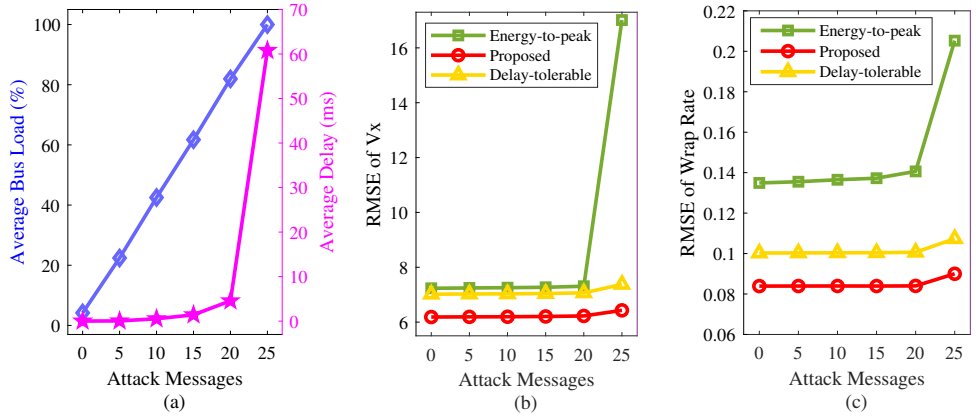

Fig. 9 Comparisons of speed tracking performance and oscillation damping capability of different control strategies with the increase of replay attack messages in the presence of actuator saturation: (a) Average bus load and average delay, (b) RMSE of Vx, (c) RMSE of wrap rate.

values of speed tracking and wrap rate of the proposed controller are the smallest under different attack energies, compared with delay-tolerable and energy-to-peak controller. It shows that proposed method has the superiority speed tracking performance and oscillation damping capability under different attack energies with input saturation. 3) The increase of attack energy has the greatest influence on the energy-to-peak controller, followed by the delay-tolerable controller, and finally the proposed controller. Therefore, the proposed controller show its strong stability against bus load and communication delay changes. In the future, more control problems under multi-domain boundary conditions are expected to be studied. Besides, solving nonlinear matrix inequality problems is also a point worthy of future research.

Acknowledgements This work is financially supported by the National Natural Science Foundation of China (Grant Number: 52172352), Key Science and Technology Innovation Project of Shandong Province (Grant Number: 2019JZZY010913), 2025 Science and Technology Innovation Program of Ningbo (Grant Number: 2020Z026, 2020Z027, 2020Z028), Key Science and Technology Project of Guangxi Province (Grant Number: AA19254013) and Primary Research and Development Plan of Zhejiang Province (Grant Number: 2021C01140).

Data availability

The data that support the findings of this study are available from the corresponding author upon reasonable request.

Conflict of interest

The authors declare that they have no conflict of interest.

References

1. Ahmed, A., Rehan, M., Iqbal, N.: Delay-dependent anti-windup synthesis for stability of constrained state delay systems using pole-constraints. ISA transactions **50**(2), 249–255 (2011). Https://doi.org/10.1016/j.isatra.2010.11.003
2. Akram, A., Hussain, M., Rehan, M., et al.: Dynamic anti-windup compensation of nonlinear time-delay systems using lpv approach. Nonlinear Dynamics **90**(1), 513–533 (2017). Https://doi.org/10.1007/s11071-017-3678-8
3. Alnasser, A., Sun, H.: Trust-based model for securing vehicular networks against rsu attacks. In: IEEE INFOCOM 2021-IEEE Conference on Computer Communications Workshops (INFOCOM WKSHPS), pp. 1–6. IEEE (2021). Https://doi.org/10.1109/infocomwkshps51825.2021.9484458
4. Cao, Y.Y., Wang, Z., Tang, J.: Analysis and anti-windup design for time-delay systems subject to input saturation. In: 2007 International Conference on Mechatronics and Automation, pp. 1968–1973. IEEE (2007). Https://doi.org/10.1109/icma.2007.4303852
5. Chen, Y., Fei, S., Zhang, K.: Stabilization of impulsive switched linear systems with saturated control input. Nonlinear Dynamics **69**(3), 793–804 (2012). Https://doi.org/10.1007/s11071-011-0305-y
6. Chen, Y., Yang, M., Liu, K., Long, J., Xu, D., Blaabjerg, F.: Reversed-structure-based pi-lead controller anti-windup design and self-commissioning strategy for servo drive systems. IEEE Transactions on Industrial Electronics (2021). Https://doi.org/10.1109/tie.2021.3097602
7. Chen, Z., Liu, Y., Fu, Y., Xu, X.: Motor-torque-limited power-on upshift control in electric vehicles with automatic transmissions. Proceedings of the Institution of Mechanical Engineers, Part D: Journal of Automobile Engineering **230**(1), 18–36 (2016). Https://doi.org/10.1177/0954407015577309

8. Da Suva, J., Tarbouriech, S., Garcia, G.: Using anti-windup loops for enlarging the stability region of time-delay systems subject to input saturation. In: Proceedings of the 2004 American Control Conference, vol. 5, pp. 4819–4824. IEEE (2004). Https://doi.org/10.23919/acc.2004.1384076
9. Dong, P., Zuo, S., Du, S., Tenberge, P., Wang, S., Xu, X., Wang, X.: Optimum design of the tooth root profile for improving bending capacity. Mechanism and Machine Theory **151**, 103910 (2020). Https://doi.org/10.1016/j.mechmachtheory.2020.103910
10. Groza, B., Murvay, P.S.: Security solutions for the controller area network: Bringing authentication to in-vehicle networks. IEEE Vehicular Technology Magazine **13**(1), 40–47 (2018). Https://doi.org/10.1109/mvt.2017.2736344
11. Guo, J., Luo, Y., Li, K.: Adaptive neural-network sliding mode cascade architecture of longitudinal tracking control for unmanned vehicles. Nonlinear Dynamics **87**(4), 2497–2510 (2017). Https://doi.org/10.1007/s11071-016-3206-2
12. Han, M., Cheng, P., Ma, S.: Ppm-invids: Privacy protection model for in-vehicle intrusion detection system based complex-valued neural network. Vehicular Communications **31**, 100374 (2021). Https://doi.org/10.1016/j.vehcom.2021.100374
13. Hu, T., Teel, A.R., Zaccarian, L.: Anti-windup synthesis for linear control systems with input saturation: Achieving regional, nonlinear performance. Automatica **44**(2), 512–519 (2008). Ttps://doi.org/10.1016/j.automatica.2007.06.003
14. Hussain, M., Muslim, F.B., Khan, O., et al.: Robust anti-windup control strategy for uncertain nonlinear system with time delays. Arabian Journal for Science and Engineering pp. 1–14 (2021)
15. Hussain, M., Rehan, M., Ahn, C.K., Zheng, Z.: Static anti-windup compensator design for nonlinear time-delay systems subjected to input saturation. Nonlinear Dynamics **95**(3), 1879–1901 (2019). Https://doi.org/10.1007/s11071-018-4666-3
16. Karl, K., Alexei, C., Franziska, R.: Experimental security analysis of a modern automobile. In: 31st IEEE Symposium on Security and Privacy, S&P 2010, 16-19 May 2010, Berleley/Oakland, California, USA, pp. 447–462. IEEE (2010). Https://doi.org/10.1109/vtcfall.2018.8690781
17. Lee, S., Kwon, O., Park, J.H.: Regional asymptotic stability analysis for discrete-time delayed systems with saturation nonlinearity. Nonlinear Dynamics **67**(1), 885–892 (2012). Https://doi.org/10.1007/s11071-011-0032-4
18. Li, W., Zhu, W., Zhu, X., Guo, J.: Robust oscillation suppression control of electrified powertrain system considering mechanical-electric-network effects. IEEE Access **8**, 56441–56451 (2020). Https://doi.org/10.1109/access.2020.2982317
19. Li, X., Xu, X., Zhang, H., Dong, P., Liu, Y.: Dos-robust dynamic speed tracking controller for an integrated motor-gearbox powertrain system of a connected car. In: 2019 3rd Conference on Vehicle Control and Intelligence (CVCI), pp. 1–6 (2019). Https://doi.org/10.1109/cvci47823.2019.8951593
20. Liang, C., Xu, X., Wang, F., Zhou, Z.: H_∞ non-clutch coordinated control for mode transition system of dm-phev with can-induced delays. Nonlinear Dynamics pp. 1–19 (2021). Https://doi.org/10.1007/s11071-021-07004-y
21. Lozier, J.: A steady state approach to the theory of saturable servo systems. IRE Transactions on Automatic Control **1**(1), 19–39 (1956). Https://doi.org/10.1109/tac.1956.1100815
22. Lu, N., Cheng, N., Zhang, N., Shen, X., Mark, J.W.: Connected vehicles: Solutions and challenges. IEEE internet of things journal **1**(4), 289–299 (2014)
23. Luo, F., Hu, Q.: Security mechanisms design for in-vehicle network gateway. Tech. rep., SAE Technical Paper (2018). Https://doi.org/10.4271/2018-01-0018
24. Mane, V., Iyer, N.C.: Enhanced safety and security features for can communication in automotives. In: Information and Communication Technology for Competitive Strategies (ICTCS 2020), pp. 215–225. Springer (2021). Https://doi.org/10.1007/978-981-16-0882-7
25. Naamane, K., Tissir, E.H.: Robust anti-windup controller design for takagi–sugeno fuzzy systems with time-varying delays and actuator saturation. Circuits, Systems, and Signal Processing **41**(3), 1426–1452 (2022)
26. Pal-Stefan, M., Bogdan, G.: Security shortcomings and countermeasures for the SAE J1939 commercial vehicle bus protocol. IEEE Transactions on Vehicular Technology **67**(5), 4325–4339 (2018). Https://doi.org/10.1109/tvt.2018.2795384
27. Parkinson, S., Ward, P., Wilson, K., Miller, J.: Cyber threats facing autonomous and connected vehicles: Future challenges. IEEE transactions on intelligent transportation systems **18**(11), 2898–2915 (2017). Https://doi.org/10.1109/tits.2017.2665968
28. Rehan, M., Hong, K.S.: Decoupled-architecture-based nonlinear anti-windup design for a class of nonlinear systems. Nonlinear Dynamics **73**(3), 1955–1967 (2013). Https://doi.org/10.1007/s11071-013-0916-6
29. Shuai, Z., Zhang, H., Wang, J., Li, J., Ouyang, M.: Combined AFS and DYC control of four-wheel-independent-drive electric vehicles over CAN network with time-varying delays. IEEE Transactions on Vehicular Technology **63**(2), 591–602 (2014).

Https://doi.org/10.1109/tvt.2013.2279843
30. da Silva, J.G., Bender, F.A., Tarbouriech, S., Biannic, J.M.: Dynamic anti-windup synthesis for state delayed systems: an lmi approach. In: Proceedings of the 48h IEEE Conference on Decision and Control (CDC) held jointly with 2009 28th Chinese Control Conference, pp. 6904–6909. IEEE (2009). Https://doi.org/10.1109/cdc.2009.5399738
31. da Silva Jr, J.M.G., Tarbouriech, S., Garcia, G.: Anti-windup design for time-delay systems subject to input saturation an lmi-based approach. European Journal of Control **12**(6), 622–634 (2006)
32. Song, G., Wang, Z.: A delay partitioning approach to output feedback control for uncertain discrete time-delay systems with actuator saturation. Nonlinear Dynamics **74**(1), 189–202 (2013). Https://doi.org/10.1007/s11071-018-4666-3
33. Tae Un, K., Hyun Min, S., Seonghoon, J., Huy Kang, K.: Automated reverse engineering and attack for CAN using OBD-II. In: IEEE Vehicular Technology Conference, pp. 1–7 (2018). Https://doi.org/10.1109/vtcfall.2018.8690781
34. Uhlemann, E.: Connected-vehicles applications are emerging [connected vehicles]. IEEE Vehicular Technology Magazine **11**(1), 25–96 (2016). Https://doi.org/10.1109/mvt.2015.2508322
35. Wang, Y., Cao, Y., Sun, Y.: Anti-windup compensator gain design for time-delay systems with constraints. Acta Automatica Sinica **32**(1), 455–470 (2006). Https://doi.org/10.1016/j.neucom.2015.12.078
36. Woo, S., Jo, H.J., Kim, I.S., Lee, D.H.: A practical security architecture for in-vehicle can-fd. IEEE Transactions on Intelligent Transportation Systems **17**(8), 2248–2261 (2016). Https://doi.org/10.1109/tits.2016.2519464
37. Woo, S., Jo, H.J., Lee, D.H.: A practical wireless attack on the connected car and security protocol for in-vehicle CAN. IEEE Transactions on Intelligent Transportation Systems **16**(2), 993–1006 (2015)
38. Wu, F., Lu, B.: Anti-windup control design for exponentially unstable lti systems with actuator saturation. Systems & Control Letters **52**(3-4), 305–322 (2004). Https://doi.org/10.1016/j.sysconle.2004.02.007
39. Xi, L., Xiangyang, X., Yanfang, L.: Simulation of gear-shift algorithm for automatic transmission based on matlab. In: 2009 WRI World Congress on Software Engineering, vol. 2, pp. 476–480. IEEE (2009). Https://doi.org/10.1109/wcse.2009.198
40. Xu, X., Dong, P., Liu, Y., Zhang, H.: Progress in automotive transmission technology. Automotive Innovation **1**(3), 187–210 (2018). Https://doi.org/10.1007/s42154-018-0031-y
41. Xu, X., Li, X., Dong, P., Liu, Y., Zhang, H.: Robust reset speed synchronization control for an integrated motor-transmission powertrain system of a connected vehicle under a replay attack. IEEE Transactions on Vehicular Technology **70**(6), 5524–5536 (2020). Https://doi.org/10.1109/tvt.2020.3020845
42. Xu, X., Li, X., Zhang, H., Zhou, J.: Event-triggered robust control of an integrated motor-gearbox powertrain system for a connected vehicle under can and dos-induced delays. In: SAE 2019 Intelligent and Connected Vehicles Symposium. SAE International (2020). Https://doi.org/10.4271/2020-01-5016
43. Yang, D., Jiang, K., Zhao, D., Yu, C., Cao, Z., Xie, S., Xiao, Z., Jiao, X., Wang, S., Zhang, K.: Intelligent and connected vehicles: Current status and future perspectives. Science China Technological Sciences **61**(10), 1446–1471 (2018). Https://doi.org/10.1007/s11431-017-9338-1
44. Zhang, C., Zhang, Q., He, J., Liu, J., Yang, X., Mao, S.: Consistent total traction torque-oriented coordinated control of multimotors with input saturation for heavy-haul locomotives. Journal of Advanced Transportation **2020** (2020)
45. Zhao, J., Shen, H., Li, B., Wang, J.: Finite-time H_∞ control for a class of markovian jump delayed systems with input saturation. Nonlinear Dynamics **73**(1), 1099–1110 (2013). Https://doi.org/10.1007/s11071-013-0855-2
46. Zhao, Y., Xu, J.: Using the delayed feedback control and saturation control to suppress the vibration of the dynamical system. Nonlinear Dynamics **67**(1), 735–753 (2012). Https://doi.org/10.1007/s11071-011-0023-5
47. Zhu, X., Zhang, H., Cao, D., Fang, Z.: Robust control of integrated motor-transmission powertrain system over controller area network for automotive applications. Mechanical Systems and Signal Processing **58**, 15–28 (2015). Https://doi.org/10.1016/j.ymssp.2014.11.011